Ferromagnetic resonance and resonance modes in kagome lattices: From an open to a closed kagome structure

J. Dubowik,* P. Kuświk, M. Matczak, W. Bednarski, and F. Stobiecki
Institute of Molecular Physics, Polish Academy of Sciences, M. Smoluchowskiego 17, PL-60-179 Poznań, Poland

P. Aleshkevych and H. Szymczak
Institute of Physics, Polish Academy of Sciences, Al. Lotników 32/46, PL-02-668 Warszawa, Poland

M. Kisielewski and J. Kisielewski
Faculty of Physics, University of Białystok, K. Ciołkowskiego 1L, PL-15-245 Białystok, Poland
(Received 27 January 2016; revised manuscript received 29 April 2016; published 22 June 2016)

We present ferromagnetic resonance (FMR) investigations of 20 nm thick permalloy ($Ni_{80}Fe_{20}$) elements (width $W = 200$ nm, length $L = 470$ nm, period $a = 500$ nm) arranged in open and closed artificial kagome lattices. The measurements were done at 9.4 and 34 GHz to ensure a saturated or near-saturated magnetic state of the kagome structures. The FMR data are analyzed in the framework of an analytical macrospin model which grasps the essential features of the bulk and edge modes at these microwave frequencies and is in agreement with the results of micromagnetic simulations. Polar plots of the resonance fields versus the field angle made by the direction of the magnetic field with respect to the main symmetry directions of the kagome lattice are compared with the results of the analytical model. The measured FMR spectra with a sixfold rotational symmetry qualitatively reproduce the structure expected from the theory. Magnetic dipolar interactions between the elements of the kagome lattices result in the mixing of edge and bulklike excitations at 9.4 GHz and in a systematic deviation from the model, especially for the closed kagome lattice.

DOI: 10.1103/PhysRevB.93.224423

I. INTRODUCTION

Advances in nanolithography make it possible to pattern ferromagnetic films into various types of two-dimensional (2D) lattices (square [1], triangular [2], honeycomb [3], kagome [4], or even quasicrystalline [5] or fractal [6] lattices) in which each element is small enough to be a single-domain nanoparticle. The magnetic energy F of an array of the elements

$$F = \frac{1}{2}\sum_{i\neq j}\left\{\frac{(\vec{m}_i\cdot\vec{m}_j)}{r_{ij}^3} - \frac{3(\vec{m}_i\cdot\vec{r}_{ij})(\vec{m}_j\cdot\vec{r}_{ij})}{r_{ij}^5}\right\} + \frac{1}{2}\sum_i\left\{N_{xi}m_{xi}^2 + N_{yi}m_{yi}^2 + N_{zi}m_{zi}^2\right\} - \sum_i(\vec{m}_i\cdot\vec{H}_{\rm ex}) \quad (1)$$

is described by interactions between the magnetic moments m_i, m_j of the ith and jth particles separated by r_{ij} and their interactions with an external magnetic field $H_{\rm ex}$, and depends on their shape through demagnetizing factors N_{xi}, N_{yi}, and N_{zi} along their main axes.

In such systems, the competition between the Zeeman energy [the third term in Eq. (1)], the shape anisotropy of the individual nanoelements (the second term), and magnetostatic interactions (the first term) results in a symmetry of the spin wave (SW) spectra, including configurational anisotropy [7,8].

Ferromagnetic resonance (FMR) studies have shown a high sensitivity of the SW spectra to the geometry, separation, and edge imperfections, as well as a dynamic dipolar coupling [9] tuned by the complexity of the magnetization pattern [6]. In sets of triangular nanorings, FMR spectra with multiple resonance peaks showing a sixfold symmetry were validated using a modified Kittel equation and micromagnetic simulations [2]. The same group of authors characterized the eigenmode spectra in arrays consisting of noncollinearly arranged magnetic rectangular elements [10]. They found two distinct collective FMR modes and explained them as predominantly localized in elements with different easy-axis orientations. Additionally, angular FMR measurements confirmed a fourfold rotational symmetry for the array due to combination of two (perpendicular to each other) uniaxial configurational anisotropies. FMR spectra acquired for various directions of an applied magnetic field in aperiodic wire networks on Fibonacci distortions of square antidot lattices exhibit a fourfold rotational symmetry [11] but with a more complex behavior than comparable periodic square antidote lattices [12]. In quasicrystalline Ammann tailings, FMR spectra exhibit an eightfold rotational symmetry [13]. Finally, in quasicrystalline Penrose tailings (P2T) with a fivefold symmetry, FMR spectra exhibit a tenfold rotational symmetry [5].

In most cases, micromagnetic simulations have been shown to give access to the spatially resolved magnitudes of magnetization precession, so that various SW modes [5,6] can be identified, including even exotic excitations due to the presence of magnetic monopoles or Dirac strings [14]. Specifically, it has been found that the topological defects in artificial spin-ice lattices display distinct signatures in an SW mode spectrum of square spin-ice lattices, providing a means to qualitatively and quantitatively analyze monopoles and strings that can be measured experimentally [14]. These defects have been also observed in kagome lattices [9].

*dubowik@ifmpan.poznan.pl

Here, we investigate FMR spectra in kagome lattices. The main purpose of the paper is to provide a general description of the in-plane angular dependencies of the resonance fields $H_r(\phi_H)$ in the kagome lattices with a sixfold symmetry. Despite a series of papers that have addressed the angular dependencies of the resonance fields in relatively simple [2,6,10] or more complicated [5,11,13] magnonic structures of mesoscopic dimensions, there is a dearth of coherent and comprehensive descriptions of these dependencies. Some attempts to characterize $H_r(\phi_H)$ in a triangular lattice are notable exceptions [2], however, with no explanation of the origin of a sixfold rotational symmetry of the spectra for a lattice consisting of triangles. We show how to describe angular dependencies of the resonance fields in relatively simple kagome lattices within the framework of a macrospin model and how to combine dependencies of bulk modes with edge modes, which play an important role in spin dynamics of artificial spin-ice lattices besides modes localized on defects [14]. But besides that, the resultant polar plots of the resonance fields in kagome lattices also serve as an example of the Curie principle [15], which states that a macroscopic cause (i.e., symmetry of the kagome lattice) never has more elements of symmetry than the effect it produces (i.e., symmetry of the resonance field distribution). In other words, "A symmetry characteristic of one or another phenomenon is the highest symmetry of the medium compatible with the occurrence of this phenomenon" [16].

The individual elements of the kagome lattices may be connected in a closed structure or in an open kagome lattice, not connected. Hence, either the exchange or magnetostatic interactions are expected to have an impact on the angular dependencies of the FMR spectra. The FMR data obtained in a fully saturated state (i.e., at 34 GHz) or a nearly saturated state (at 9.4 GHz) are analyzed with the use of micromagnetic simulations and an analytical macrospin model for the main modes confined in the bulk of the nanoelements (bulk, center modes) as well as modes localized at the edges (edge modes). In the macrospin model, the first term in Eq. (1) is neglected. Therefore it is an independent particle (element) approach. However, some salient characteristics of the experimental angular dependencies of the resonance field (presented in this paper as polar plots) can be ascribed to dipolar interactions between the elements.

II. EXPERIMENTAL DETAILS AND MICROMAGNETIC SIMULATIONS

A set of permalloy ($Ni_{80}Fe_{20}$) kagome lattices with a thickness of 20 nm were fabricated using magnetron sputtering and liftoff techniques. A thin layer of polymethyl methacrylate positive resist was spin-coated onto naturally oxidized Si(100) substrates and then patterned with a Raith 50 electron-beam lithography writer into open or closed kagome patterns and, after development, a permalloy film was deposited and the patterns were lifted off using sonication in acetone. The approximate length, width, and thickness of one permalloy stadium is $L = 470$ nm, $W = 200$ nm, and $t = 20$ nm, respectively Fig. 1(a). In the open structure, the elements are separated by 20–30 nm so that they interact with each other via dipolar interactions. In the closed structures Fig. 1(c) the elements are in contact and form an antidot structure. They will be discussed later in Sec. IV C. FMR measurements were performed at the microwave frequencies 9.4 GHz and 34 GHz and dc applied magnetic fields $0 < H < 3$ kOe and $0 < H < 15$ kOe, respectively, using standard microwave

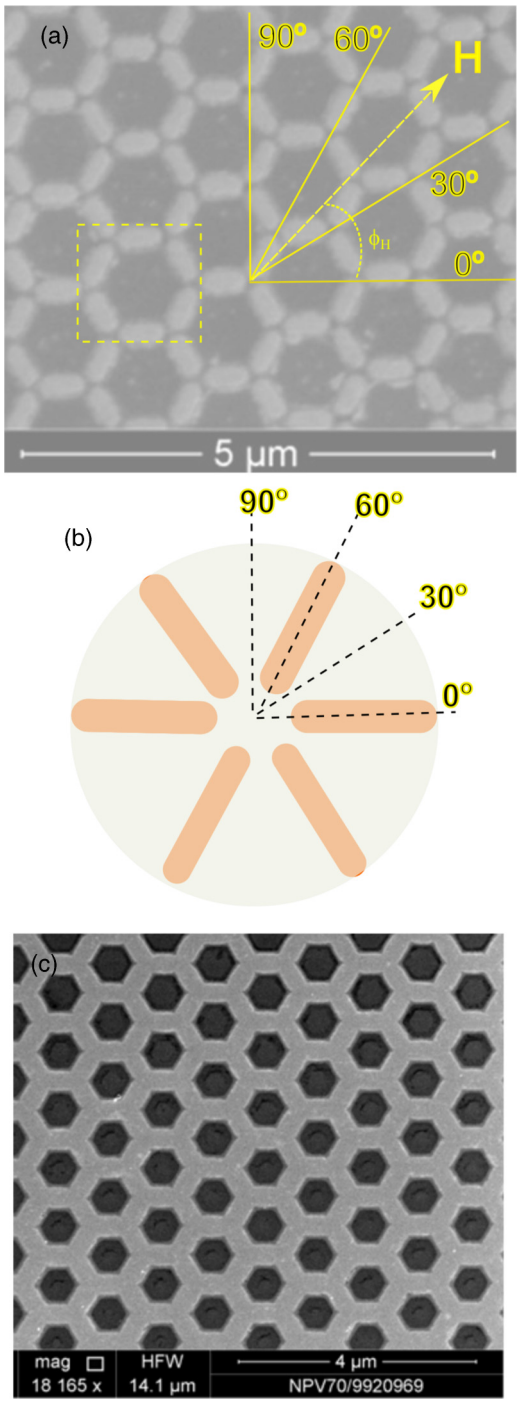

FIG. 1. The artificial kagome lattice. (a) Scanning electron microscope image of an open kagome structure fabricated from 20 nm thick permalloy elements (width $W = 200$ nm, length $L = 470$ nm, period $a = 500$ nm). (b) Schematic configuration of orientation of the elements within a macrospin approach. (c) Scanning electron microscope image of a closed kagome structure with approximately the same dimensions.

cavities. In all FMR experiments, the dc field could be rotated within the film plane by an angle ϕ_H between H and a reference edge of the kagome [0° axis shown in Fig. 1(a)]. Static magnetization measurements performed using a Kerr magnetometer gave a coercive force of 300 Oe.

Dynamic FMR data were simulated using the Object Oriented Micromagnetic Framework (OOMMF) code [17] with periodical boundary conditions for a unit kagome cell 1.79×2.065 μm. We used the basic OOMMF package for which finite temperature is not taken into account. All simulations were performed at zero temperature. The accreditation cell sizes were $5 \times 5 \times 10$ nm^3. For a given magnetic field the magnetization was allowed to come to equilibrium and then disturbed with a short pulse that rotated the magnetization away from equilibrium. The magnetization was then allowed to evolve using the Landau-Lifshitz-Gilbert equation. The resulting magnetization oscillations were Fourier transformed to obtain a power spectrum with peaks corresponding to the resonances of the kagome structure in a given field oriented in a given direction. Identification of the various bulk and edge modes was achieved through mode imaging.

As can be seen in Fig. 1(b), all stadium nanoelements are arranged in a kagome lattice in a sixfold symmetry with the main directions at $0° + n \times 60°$ with $n = 0, 1, \ldots, 5$. When H is applied at $\phi_H = 0° + n \times 60°$ there are two elements magnetized along the long axis (i.e., the easy direction of the element) and the other four elements are magnetized at $\pm 60°$ (at 60° for short) with respect to the direction of H. When H is applied at $\phi_H = 30° + n \times 60°$, there are two elements magnetized along the short axis (i.e., the hard direction of the element) and the other four elements are magnetized at $\pm 30°$ (30° for short) with respect to the applied magnetic field.

The FMR measurements at 9.4 GHz were performed at 5 K and 300 K, and those at 34 GHz were performed at 300 K. Typical resonance spectra at 34 and 9.4 GHz of the open structure are shown in Figs. 2(a) and 2(b), respectively. The spectra are rather complex, with 3–4 intensive modes, depending on the orientation, and some additional weaker modes, which are most clearly seen in Fig. 2(b): 9.4 GHz at 300 K. A broad mode seen in Fig. 2(a) centered at 12 kOe is due to resonance cavity background so that the higher field modes seen at ~13–14 kOe cannot be definitely resolved.

OOMMF mode imaging of spatially resolved precessional magnitude of the magnetization at a resonance frequency for a given field value gives the answer to how to connect the observed modes with specific magnetization oscillations in the nearly decoupled single elements. Let us recall that the OOMMF simulations are conducted in a frequency-swept mode at 9 kOe [and at 1 kOe (not shown)] in contrast to the FMR experiments, which were performed in a field-swept mode at 34 and 9.4 GHz. In Fig. 3 the mode profiles in the elements are assigned to the respective simulated frequency modes for a magnetic field of 9 kOe directed at $\phi_H = 60°$ and $\phi_H = 30°$. The value of the applied magnetic field of 9 kOe was chosen since it is the mean value of the resonance fields observed in the FMR measurements taken at 34 GHz, Fig. 2(a). As confirmed by the micromagnetic simulations, this external magnetic field is strong enough to fully saturate the magnetization in the elements except for minute parts at their edges, when they are magnetized along their short axes.

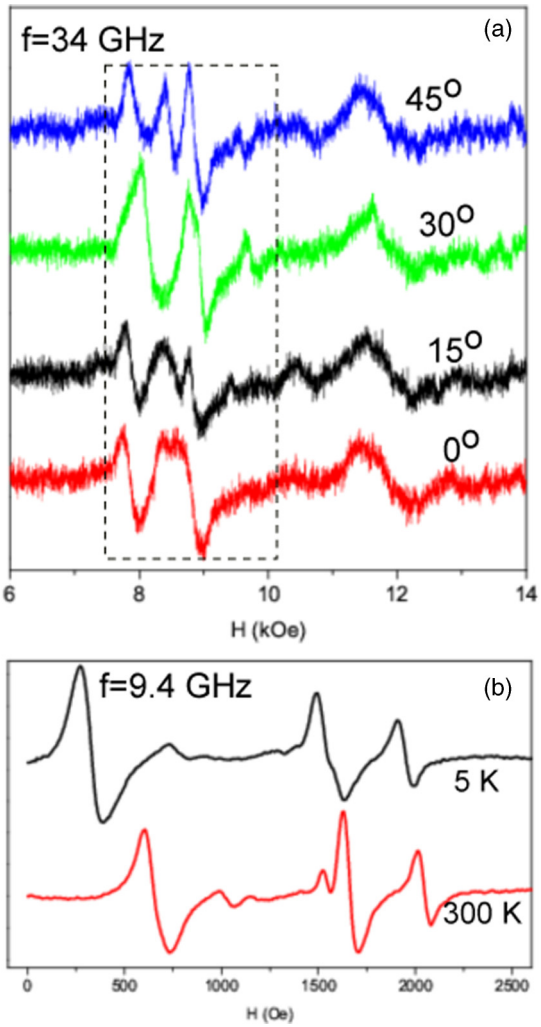

FIG. 2. (a) FMR spectra for various angles of the applied field H in kagome lattices: 34 GHz at 300 K. Dashed rectangle depicts region of interest outside cavity background centered at ~12 kOe. Dashed rectangle depicts region of interest outside a wide signal centered at 12 kOe from a resonance cavity. (b) FMR spectra for H applied at ~30°: 9.4 GHz at 5 K and 300 K.

For $\phi_H = 30°$ a mode at 34.95 GHz corresponds to nearly uniform excitations in the centers of the elements magnetized along their long axes, while a mode at 35.53 GHz is due to excitations of the elements magnetized at 60° with respect to direction of the field. For H directed at $\phi_H = 30°$, the mode at 35.20 GHz corresponds to nearly uniform oscillations in the interior of the elements magnetized along their short axes. The higher frequency modes at 36.75 and 37.28 GHz are due to SW excitations in the elements magnetized at $\phi = 30°$ with respect to the field direction. We conclude that our simulations clearly show that the macrospin model can be a good approximation for SW excitations in the interior of an element which at a high magnetic field of 9 kOe is almost fully saturated. The low-frequency modes at 31.69 and 33.48 GHz can be assigned to "trapped spin waves" or edge modes, which are typical of localized oscillations at the edges of the elements and will be also discussed in the framework of the macrospin model [18]. Further on, we will consider mostly the high-frequency edge

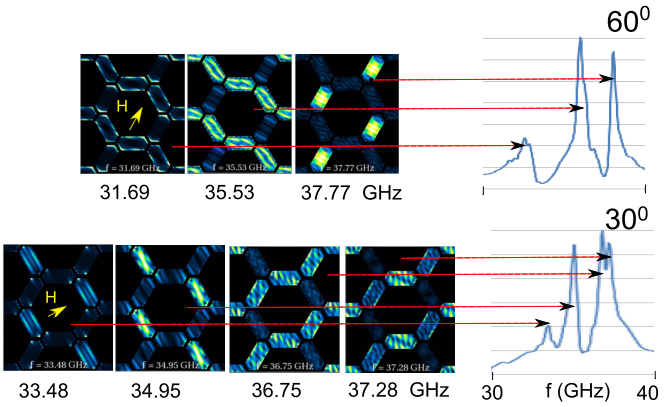

FIG. 3. Left panel: Simulated main modes in the open kagome lattice for the magnetic field of 9 kOe directed in the two main directions $\phi_H = 60^\circ$ and $\phi_H = 30^\circ$. The brighter colors (from yellow to blue) correspond to greater mode amplitudes. Right panel: Simulated FMR spectra corresponding to the modes in the left panel in the frequency domain.

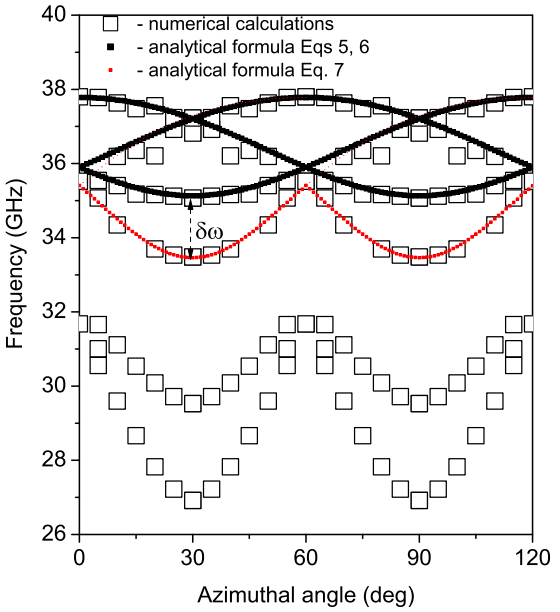

FIG. 4. Dependence of the resonance frequencies as a function of ϕ_H for the open kagome lattice at $H = 9$ kOe. Open squares: Resonance frequency obtained from numerical simulations using OOMMF. Black and red lines: The result of calculations according to Eqs. (5) and (6) and Eq. (7) for the bulk and edge modes, respectively. $\delta\omega$ is the difference between the resonance frequencies of the edge and bulk modes at $\phi_H = 30^\circ$. Lower frequency edge modes at 31–25 GHz will not be discussed further, since they have low intensities in the simulated spectra.

modes (similar to those at 33.48 GHz, i.e., at fields of 9 kOe) which are accessible to our field-swept FMR experiments. The low-frequency edge modes (like those at 31.69 GHz) will not be discussed further since they lie in between 11 and 14 kOe in FMR measurements at 34 GHz, where they are obscured by the cavity background. However, as can be seen in Fig. 2(a), in the field-swept FMR measurements at 34 GHz there are some modes (at ∼11 and 13 kOe) that are presumably related to these higher order edge modes.

III. MACROSPIN MODEL

The values of the resonance frequency estimated from OOMMF simulations for the open kagome lattice as a function of the azimuthal angle ϕ_H are shown in Fig. 4 as the open squares. In accordance with the symmetry of the kagome lattice (Fig. 1) the variation of the resonance frequency as a function of ϕ_H exhibits sixfold rotational symmetry due to the kagome lattice geometry. From an analysis of simulated mode profiles (Fig. 3, left panel) the modes spanning a frequency range from ∼35 to ∼38 GHz are the bulklike modes with nearly uniform oscillations of the magnetization in the interior of the elements. As mentioned above, the modes covering a lower frequency range (i.e., 26 to 35 GHz) are the edge modes. Since the intensities of the edge modes with frequencies spanning a range of 26–32 GHz are lower than the dominating bulklike modes, they will not be analyzed further except for the lowest edge mode with frequencies spanning a range of 35–33 GHz.

Let us describe the ferromagnetic resonance in the open kagome lattice in the framework of an independent grain approach, which assumes no coupling between the grains. Therefore, the resonance spectra of the lattice are the sum of the individual responses of all elements with a specific magnetization configuration that depends on the strength of the applied magnetic field H and the azimuthal angle ϕ_H. For a single element with demagnetizing factors N_x, N_y, N_z ($N_x + N_y + N_z = 1$ and $N_z \gg N_y > N_x$), the free energy F consists of the Zeeman and demagnetizing energy terms

$$F = -HM\sin\Theta\cos(\phi - \phi_H) + 2\pi M^2[N_x \sin^2\Theta\cos^2\phi + N_y \sin^2\Theta\sin^2\phi + N_z\cos^2\Theta], \quad (2)$$

where M is the magnetization and ϕ, Θ are the azimuthal and polar angles of the magnetization, respectively. Assuming that H is applied in the plane of the elements ($\Theta = 90^\circ$), the equilibrium condition for magnetization is

$$H\sin(\phi - \phi_H) + 2\pi M\Delta N_{yx}\cos 2\phi = 0, \quad (3)$$

where $\Delta N_{yx} = N_y - N_x$. The corresponding resonance angular frequency $\omega = 2\pi f$ (f is the microwave frequency in GHz) can be easily obtained using Smit's relation [19] and is

$$\omega = \gamma\{[H\cos(\phi - \phi_H) + 4\pi M(N_z - N_x - \Delta N_{yx}\sin^2\phi)] \times [H\cos(\phi - \phi_H) + 4\pi M\Delta N_{yx}\cos 2\phi]\}^{1/2}, \quad (4)$$

where γ is the gyromagnetic ratio. It is easy to show that for the field orientation along the principal element axes x and y, Eq. (4) is equivalent to the Kittel equations with the appropriate N_x, N_y, N_z determined in the simplest [20] form by the geometry of the single elements by $N_x = \frac{t/L}{1+t/L+t/W}$, $N_y = \frac{W/L}{1+t/L+t/w}$, $N_z = \frac{1}{1+t/L+t/W}$. For our permalloy elements (see Fig. 1), the corresponding demagnetizing factors are 0.035, 0.086, and 0.875 but in reality they may differ slightly since the simulated mode profiles of magnetization excitations (see Fig. 3) differ from those of a uniformly magnetized element. Since in the independent element approach we have

six elements in a unit cell (Fig. 1), we can introduce into Eqs. (4) and (3) the angles $\phi_U = 0°, 60°, 120°, 180°, 240°$, and 300° to label an element oriented at ϕ_U with respect to the x axis in Fig. 1(a):

$$\omega = \gamma\{[H\cos(\phi-\phi_H) + 4\pi M(N_z - N_x - \Delta N_{yx}\sin^2(\phi+\phi_U))] \times [H\cos(\phi-\phi_H) + 4\pi M\Delta N_{yx}\cos 2(\phi+\phi_U)]\}^{1/2} \quad (5)$$

and

$$H\sin(\phi-\phi_H) + 2\pi M\Delta N_{yx}\cos 2(\phi+\phi_U) = 0. \quad (6)$$

These two relations describe the dependence of the resonance frequency (field) on the angle ϕ_H for bulk quasiuniform modes which extend into the interior of the elements.

A dispersion relation similar to Eq. (5) can be derived for the edge modes which are confined on the long edges of the elements:

$$\omega = \gamma\left(\left[H + 4\pi M\tilde{N}\left(1 - \tfrac{3}{2}\sin^2\phi_H\right)\right] \times \left\{H + 4\pi M\left[1 - \tilde{N}\left(\tfrac{3}{2} - \tfrac{1}{2}\cos 2\phi_H\right)\right]\right\}\right)^{1/2}. \quad (7)$$

$\tilde{N}$ plays the role of an effective demagnetizing factor in the macrospin approximation of the edge modes, and is of the order of $t/(t+d_e)$, where d_e is the edge mode depth [18]. To simplify Eq. (7), we assume that $\phi = \phi_H$ since the edge modes occur for the field H applied perpendicularly (or near perpendicularly) to the edge, i.e., $\phi_H = \phi = 30° + n \times 60°$. Note that for $\phi_H = 90°$, Eq. (7) is the same as Eq. (4) in Ref. [18] and for $\phi_H = 0°$, it has the same form as Eq. (1) in Ref. [21] for longitudinally magnetized stripes. In our analysis of the simulated data N_x, N_y, N_z, and $\tilde{N}$ can be treated as fitting parameters. The best fits are with $N_x = 0.015$, $N_y = 0.10$, $N_z = 0.885$, and $\tilde{N} = 0.18$, and are shown in Fig. 4 assuming $M = 800$ G and a gyromagnetic ratio of $\gamma/2\pi = 2.9$ MHz/Oe, which are typical for permalloy [20]. The lower frequency edge modes seen in Fig. 4 can be ascribed to $\tilde{N} = 0.28$–0.3 and $\tilde{N} = 0.35$–0.36. The values of the dynamical demagnetizing factors N_x, N_y, N_z differ from those of the static demagnetizing factors calculated from the geometry of the elements constituting the open kagome lattice (i.e., $N_x = 0.035$, $N_y = 0.086$, and $N_z = 0.875$). Possible causes of this discrepancy have been discussed in Ref. [2]. As to outline to what degree the model of independent elements estimates a difference between the resonance fields of the edge and bulk modes for $\phi_H = 30° \pm 20° + n \times 60°$, it is easy to approximate this difference as

$$\delta H(\phi_H) = H_{edge}(\phi_H) - H_{bulk}(\phi_H) \approx 2\pi M[(2\tilde{N} - 3N_{yx})\sin^2(\phi_H + n \times 60°) - 3N_x], \quad (8)$$

making use of Eqs. (5) and (7). The maximal value of δH is thus

$$\delta H(30° + n \times 60°) \approx 2\pi M(2\tilde{N} - 3N_y). \quad (9)$$

For the simulated data shown in Fig. 4 the difference between the edge and bulk mode frequencies is $\delta\omega = 1.8$ GHz, which gives approximately $\delta H \simeq \delta\omega/2.9$ MHz/Oe $\simeq$620 Oe with $\tilde{N} = 0.21$ and $N_y = 0.10$. This value does not differ much from the experimental value of $\delta H = 750$ Oe obtained from the experiment at 34 GHz (Fig. 5) with $N_y = 0.11$, $\tilde{N} = 0.24$, and $2\pi M = 5$ kOe, Eq. (8).

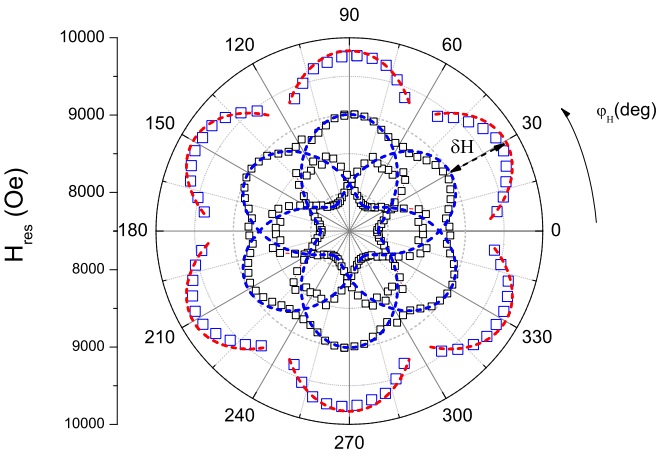

FIG. 5. Polar plot of resonance fields as a function of ϕ_H at 34 GHz and $T = 300$ K. Open squares: Data points. Blue and red lines: The result of calculations according to Eqs. (5) and (6) and Eq. (7), respectively. δH is the difference between the resonance fields of the edge and bulk modes at $\phi_H = 30°$.

IV. FMR RESULTS AND DISCUSSION

A. FMR at 34 GHz

As shown in Fig. 5, for angular measurements of $H_r(\phi_H)$ at 34 GHz the values of the resonance field as a function of angle ϕ_H can be plotted in a convenient way as a polar plot. As can be expected, a sixfold symmetry of the resonance fields is clearly seen. At 34 GHz, the external magnetic field of 8–10 kOe is high enough to magnetically saturate all elements of the kagome lattice. It can be seen that the resonance fields as a function of ϕ_H for the open kagome lattice (open squares) can be satisfactorily described within the macrospin model both for the bulk modes (dashed blue lines) and the edge modes (dashed red lines). A fit according to Eqs. (5) and (6) to the resonance fields of the bulk modes, already discussed in Sec. III, reproduces the experimental data with $N_x = 0.01$, $N_y = 0.11$, $N_z = 0.88$ as the fitting parameters. Since they differ from the static demagnetizing factors, they may be regarded as mode-specific dynamic demagnetizing factors [22]. The edge modes, which attain the maximal values of resonance field of 10 kOe for $\phi_H = 30° + n \times 60°$ ($n = 0, 1, \ldots, 5$) can be fitted with $\tilde{N} = 0.24$. They disappear abruptly at $\phi_H \approx 10° + n \times 60°$. As has already been observed in permalloy stripes [18], the edge modes smoothly convert to the bulk mode when the applied field is rotated away from the normal to the edges of about 40°. However, in the case of the open kagome lattice, the disappearance of the edge modes localized at the long edges is rather abrupt, as if they "jump" to the edge modes localized at the short edges of the stadiums. They can be seen as the faint edge modes localized at the short edges for $\phi_H = 60°$ in the upper panel in Fig. 3. We expect that this abrupt transformation in the edge mode is a "fingerprint" of the dipolar interactions between the elements still present at the relatively high magnetic fields. If one considers, in accordance

with Fig. 3, the edge modes which extend by $d_e \sim 100$ nm, the demagnetizing factor $\tilde{N}$ is $\frac{1}{2}\frac{t}{t+d_e} = 0.083$. This is exactly the value which one should expect for a mode located at ~8.5 kOe for $\phi_H = 0^\circ + n \times 60^\circ$ in Fig. 5 and Fig. 2(a) in the bottom spectrum taken at $\phi_H = 0^\circ$.

To sum up, at 34 GHz, the macrospin model for nearly independent stadium elements satisfactorily describes the angular dependencies of the resonance field for the open kagome lattices except for some irrelevant features related to edge modes. For $\phi_H = 30^\circ \pm 20^\circ$ we observe two bulk modes as well as one edge mode, while for $\phi_H = 60^\circ \pm 10^\circ$ there are two bulk modes and one faint edge mode located at about 8.5 kOe.

In agreement with the Curie principle, the polar plot of $H_r(\phi_H)$ from FMR measurements at 34 GHz exhibits a simple rosette shape with sixfold symmetry determined by the symmetry of the kagome lattices arranged from separated permalloy stadiums with a strong uniaxial shape anisotropy both for the edge and bulk modes. FMR spectra of the films patterned into finite quasiperiodic P2P exhibited a tenfold rotational symmetry despite a fivefold symmetry of the finite samples [5]. This feature has been explained as resulting from demagnetizing fields on the edges of third-generation decagons being too weak to break the tenfold symmetry expected for the infinite P2P. However, in view of the Curie principle the tenfold rotational symmetry of the observed FMR spectra can be seen as resulting just from superposition of parity invariance of $(M \times H)$ torque important in FMR and of the fivefold rotational symmetry of the finite P2T lattice. Hence, the symmetry of FMR spectra of finite quasiperiodic P2P (tenfold [5]) or of triangular lattices (sixfold [2]) may serve as the most spectacular examples of the Curie principle for the (odd) structural symmetry.

B. FMR at 9.4 GHz

As would be expected, a polar plot of the resonance fields as a function of ϕ_H for the open kagome lattice measured at 9.4 GHz shown in Fig. 6(a) (i.e., with the resonance fields of 0.5–2 kOe) is more complex than that at 34 GHz since the Zeeman energy is now comparable to the dipolar energy of the inter-element coupling [7]. Nonetheless, for a wide range of ϕ_H, the general shape of the $H_r(\phi_H)$ dependencies at $T = 300$ K is reproduced by the macrospin model with $N_x = 0.0375$, $N_y = 0.0875$, $N_z = 0.875$, and $\tilde{N} = 0.20$ as the fitting parameters with a noticeable deviation between the calculated resonance fields (dashed blue lines) and the experimental data points (open circles) except for the lowest resonance fields (i.e., for the elements magnetized along the long axes). This is clear: for the elements magnetized along their long axes, the vectors $\vec{M}$ and $\vec{H}$ are collinear and the magnetization is almost uniform. When the stadium-like elements have their long axes oriented at a certain angle with respect to the external field, the macrospin model of the independent elements requires that the equilibrium condition Eq. (6) be fulfilled with $\phi \neq \phi_H$ everywhere inside the elements. At 9.4 GHz (i.e., at fields of 1000 Oe) this assumption is fulfilled only approximately because of inter-element dipolar coupling. Our micromagnetic OOMMF calculations show that the magnetization at 1000 Oe is inhomogeneous, mainly at the element edges, for which stray

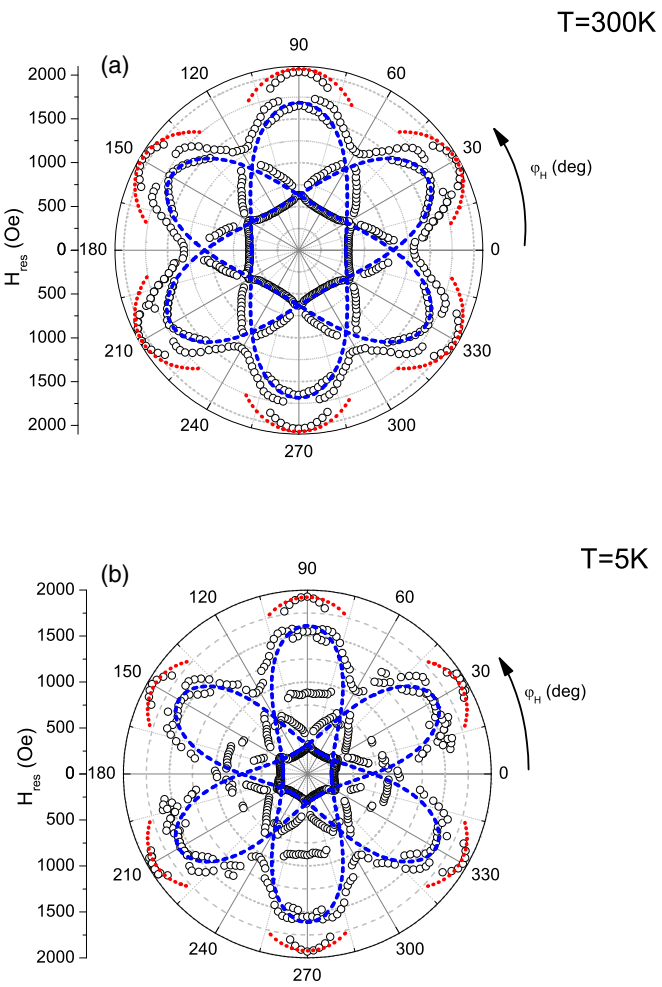

FIG. 6. Polar plots of resonance fields as a function of ϕ_H at $T = 300$ K (a) and at $T = 5$ K (b) measured at 9.4 GHz. Open symbols: Data points. Dotted (red) and dashed (blue) lines: The result of calculations of the edge and central bulk modes according to Eq. (7) and Eqs. (5) and (6), respectively.

dipolar fields play a significant role. In effect, ΔN_{yx} is almost always lower than the value assumed in the macrospin model [see Eq. (5)]. Hence, for the bulk modes $\phi - \phi_H$ is almost always lower than that in the model and the experimental resonance field H_r^{exp} is higher than the calculated resonance fields. A similar behavior can be observed at $T = 5$ K in Fig. 6(b). The differences between the 5 K and 300 K x-band data result from a higher magnetization assumed (900 G) and modified demagnetizing factors $N_x = 0.019$, $N_y = 0.086$, $N_z = 0.895$, and $\tilde{N} = 0.165$ for $T = 5$ K. However, if we compare the polar plot for $T = 300$ K with that obtained at $T = 5$ K, we clearly see that the modes at 300 K are substantially "smoothed," possibly due to thermal fluctuations of the magnetization. We have no straightforward explanation for this temperature effect but we suppose that a sort of tunneling between the modes takes place at 300 K, while at 5 K it is suppressed. Besides, it seems that some deviations from a regular sixfold symmetry seen as "individual dots" in the polar plot in Fig. 6(b) are fingerprints of a number of defected elements still present in our kagome lattice. The edge modes exist above a certain magnetic field H_{sat} of ~1200–2000 Oe for

permalloy stripes with thicknesses of 10–20 nm [18]. For this reason, at 9.4 GHz the edge modes are observed exclusively at the highest fields of 1500–2000 Oe (see Fig. 6). They exist in a limited angle range of $\pm 10^\circ$–15° from $\phi_H = 30^\circ + n \times 60^\circ$ and that their resonance fields (open symbols) decrease faster than the simulated ones (dotted red lines) as H is rotated from the normal to the long edges. This is in contrast to the mentioned behavior of the bulk modes, for which the experimental resonance fields change with the angle ϕ_H slower than those simulated. The most striking feature observed in the polar plots shown in Fig. 6(a) is the mode splitting at the angles higher than $\pm 10^\circ$ from $30^\circ + n \times 60^\circ$, i.e., where the edge modes disappear. This splitting can be explained in terms of coupled oscillations [7]. Generally, whenever there is a coupling, the energy (frequency) splits, as in coupled resonance circuits. As a result of the coupling, some modes can be regarded as mixed edge/bulk modes, and the modes with a lower resonance field as the bulklike modes. From the simulations we know that in this range of ϕ_H, magnetostatic modes with mixed characteristics can be excited: partially of the bulk type and partially of the edge type. The splitting is proportional to the coupling strength. Since the splitting seen in Fig. 6(a) is 200 Oe, we may argue that the inter-element dipolar field is of the same order ~200 Oe. A similar splitting takes place at 5 K, but we observe all bulklike and edgelike modes simultaneously, possibly because tunneling between the modes is suppressed.

Figure 7 shows in detail the behavior of the resonance fields for these modes near $\phi_H \approx 30^\circ$ at various frequencies. At 34 GHz (a) both the edge and bulk mode are excited at full saturation so that Eq. (8) is fulfilled with a difference between the resonance fields of the edge and bulk modes of $\delta H(\phi_H) \propto \sin^2(\phi_H)$ as shown in Fig. 7(d). Figure 7(b) shows that at 9.4 GHz at 300 K the edge mode exists in a narrow

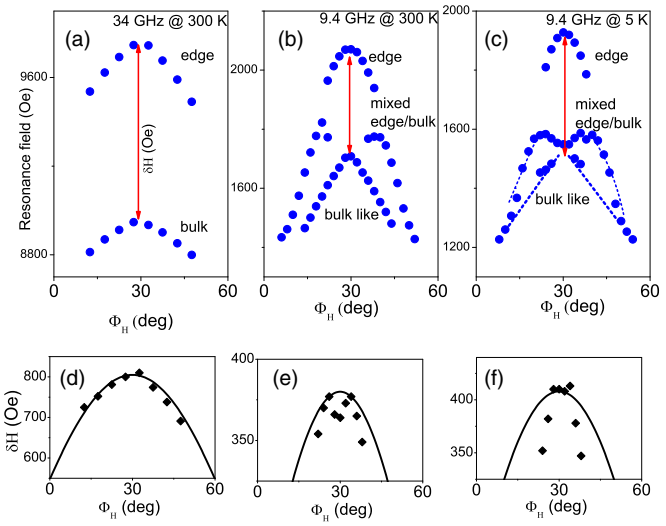

FIG. 7. Resonance fields of the edge and bulklike modes as a function of angle ϕ_H in the vicinity of $30^\circ \pm 20^\circ$ at 34 GHz (a) and 9.4 GHz at 300 K (b) and 5 K (c). Difference between the resonance field of the edge and bulk (bulklike) modes as a function of ϕ_H for the same frequencies/temperature: (d), (e), (f). Solid black lines show a trend $\propto \sin^2(\phi_H)$ according to Eq. (8).

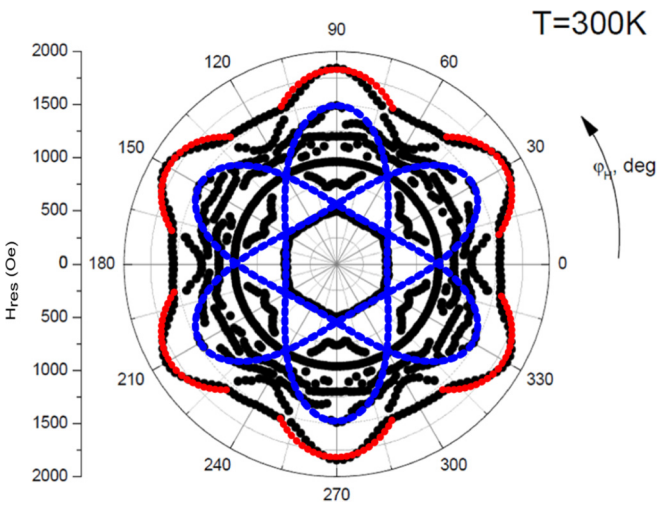

FIG. 8. Polar plots (black dots) of resonance fields for a closed kagome lattice measured at 9.4 GHz at $T = 300$ K as a function of ϕ_H. Blue and red lines show the fits to the polar plot for the open kagome lattice taken from Fig. 6(a) and scaled to the highest field of the edge mode at ~1800 Oe.

range of ϕ_H ($\pm 10^\circ$ from $\phi_H = 30^\circ$) and there is a clear splitting between the mixed edge/bulk and bulklike modes. However, since the bulklike mode is on the verge of its stability (notice that H_r vs ϕ_H has a specific triangular shape) $\delta H(\phi_H)$ decreases with ϕ_H much faster than $\sin^2(\phi_H)$ [Fig. 7(e)]. At 5 K [Fig. 7(c)] the bulklike mode exists in a very narrow range depicted by the dotted line so that the macrospin model no longer describes the spin wave excitations [Fig. 7(f)]. It is characteristic that the splitting observed at 300 K is preserved at 5 K; see Figs. 7(b) and 7(c).

C. Closed kagome lattice

As can be seen in Fig. 8, the resonance field positions in a closed kagome lattice notably differ from those of the open kagome lattices. The most important difference is that the connections in the closed kagome lattice result in an exchange coupling between the stadium elements, so that the closed kagome lattice can be regarded as a kind of antidot magnonics structure [23]. Although the FMR spectra for the closed kagome lattice show complicated structure in polar plot, we found it informative to compare the closed kagome structure experimental results with the simple macrospin model [red lines in Fig. 6(a)]. Due to the sixfold symmetry of the closed kagome lattice [Fig. 1(c)] some features characteristic of the FMR responses observed in the open kagome lattice are clearly seen in Fig. 8 as we compare the experimental data (black dots) with the fits (blue and red dotted lines) taken from Fig. 6(a). In particular, the edgelike modes behind the red dotted lines smoothly convert to bulk modes with H_r almost independent of $\phi_H \approx 0^\circ + n \times 60^\circ$ and the bulk modes with the lowest resonance fields of 500 Oe. Other modes have a substantially different behavior than that characteristic of the open kagome lattice, including a "ring" at $H_r \approx 1000$ Oe, which can be related to a uniform mode of a continuous thin film, and a lot of unresolved modes characteristic of spin wave excitations within the individual elements. Moreover, in the

closed kagome lattice, a "gap" between 500 and 750 Oe is observed with no spin wave excitations. The sixfold rotational symmetry of the FMR spectra in the closed kagome lattice is again in agreement with the Curie principle.

V. CONCLUSIONS

We have studied FMR in open and closed kagome lattices at 34 and 9.4 GHz in a field-swept mode. The results presented in this paper show how the spin wave excitations (bulklike and edgelike) in kagome lattices evolve from a fully magnetically saturated state (e.g., at 34 GHz in fields of 9 kOe) to a nearly saturated state at 9.4 GHz in fields of 1 kOe. We focus on the variations of the resonance fields on an applied field direction $H_r(\phi_H)$ for the open kagome lattice and we analyze these variations within the framework of the macrospin model. In this case, at 34 GHz, the first term in Eq. (1) is negligible in comparison with the third term.

The $H_r(\phi_H)$ obtained from FMR measurements at 9.4 GHz shows a more intricate rosette shape with a characteristic splitting due to dipolar coupling which is comparable with the third term in Eq. (1). From the splitting of the resonance field we can estimate the coupling strength to be about 200 Oe. It appears that the edge modes are the most affected by the dipole interactions, so that spin wave modes at angles higher than $\pm 10^\circ$–15° from $\phi_H = 30^\circ + n \times 60^\circ$ have a mixed edge/bulklike character. While FMR in an open kagome lattice may be approximately described in terms of the macrospin model, ferromagnetic resonance in the closed kagome lattice reveals a rich structure with a sixfold rotational symmetry still preserved in agreement with the Curie principle.

FMR at low magnetic fields would be valuable to observe other SW excitations of characteristic magnetic defects, such as monopoles or Dirac strings [14]. We tried to carry out frequency-swept FMR experiments at low fields but we failed since the sensitivity of our broad-band coplanar waveguide setup was too low. Anyway, at low fields (or in remanence) one would expect some additional SW excitations at frequencies next to that of the edge excitations. Therefore, further FMR studies at a remanence state would be valuable to check whether there is any symmetry for resonances characteristic of Dirac strings or those localized on monopoles.

ACKNOWLEDGMENTS

This work has been supported by the project "Marie Sklodowska-Curie Research and Innovation Staff Exchange (RISE)" Contract No. 644348 with the European Commission, as part of the Horizon 2020 Programme and by the SYMPHONY project operated within the Foundation for Polish Science Team Program.

[1] R. F. Wang, C. Nisoli, R. S. Freitas, J. Li, W. McConville, B. J. Cooley, M. S. Lund, N. Samarth, C. Leighton, V. H. Crespi, and P. Schiffer, Nature (London) **439**, 303 (2006).

[2] J. Ding, M. Kostylev, and A. O. Adeyeye, Appl. Phys. Lett. **100**, 062401 (2012).

[3] B. Lenk, H. Ulrichs, F. Garbs, and M. Muenzenberg, Phys. Rep. **507**, 107 (2011).

[4] E. Mengotti, L. J. Heyderman, A. Fraile Rodriguez, A. Bisig, L. Le Guyader, F. Nolting, and H. B. Braun, Phys. Rev. B **78**, 144402 (2008).

[5] V. S. Bhat, J. Sklenar, B. Farmer, J. Woods, J. T. Hastings, S. J. Lee, J. B. Ketterson, and L. E. De Long, Phys. Rev. Lett. **111**, 077201 (2013).

[6] C. Swoboda, M. Martens, and G. Meier, Phys. Rev. B **91**, 064416 (2015).

[7] V. L. Mironov, E. V. Skorohodov, and J. A. Blackman, J. Appl. Phys. **115**, 184301 (2014).

[8] R. P. Cowburn, J. Phys. D: Appl. Phys. **33**, R1 (2000).

[9] L. J. Heyderman and R. L. Stamps, J. Phys.: Condens. Matter **25**, 363201 (2013).

[10] S. Jain, M. Kostylev, and A. O. Adeyeye, Phys. Rev. B **82**, 214422 (2010).

[11] B. Farmer, V. S. Bhat, J. Sklenar, E. Teipel, J. Woods, J. B. Ketterson, J. T. Hastings, and L. E. De Long, J. Appl. Phys. **117**, 17B714 (2015).

[12] V. Bhat, J. Woods, L. D. Long, J. Hastings, V. Metlushko, K. Rivkin, O. Heinonen, J. Sklenar, and J. Ketterson, Physica C (Amsterdam, Neth.) **479**, 83 (2012).

[13] V. S. Bhat, J. Sklenar, B. Farmer, J. Woods, J. B. Ketterson, J. T. Hastings, and L. E. De Long, J. Appl. Phys. **115**, 17C502 (2014).

[14] S. Gliga, A. Kákay, R. Hertel, and O. G. Heinonen, Phys. Rev. Lett. **110**, 117205 (2013).

[15] P. Curie, J. Phys. (Paris), 3rd Ser. **3**, 393 (1894). For an English translation, see J. Rosen and P. Copié, in *Symmetry in Physics*, edited by J. Rosen (American Association of Physics Teachers, 1982), pp. 17–25.

[16] A. Shubnikov, Comput. Math. Appl. **16**, 357 (1988).

[17] D. P. M. Donahue, *OOMMF User's Guide, Version 1.0, NISTIR 6376*, Tech. Rep. (National Institute of Standards and Technology, Gaithersburg, MD, 1999).

[18] R. D. McMichael and B. B. Maranville, Phys. Rev. B **74**, 024424 (2006).

[19] J. Smit and H. G. Beljers, Philips Res. Rep. **10**, 113 (1955).

[20] C. Vittoria, *Magnetics, Dielectrics, and Wave Propagation with MATLAB Codes* (CRC Press, Boca Raton, FL, 2011).

[21] Z. Duan, C. T. Boone, X. Cheng, I. N. Krivorotov, N. Reckers, S. Stienen, M. Farle, and J. Lindner, Phys. Rev. B **90**, 024427 (2014).

[22] C. Bayer, J. Jorzick, S. Demokritov, A. Slavin, K. Guslienko, D. Berkov, N. Gorn, M. Kostylev, and B. Hillebrands, in *Spin Dynamics in Confined Magnetic Structures III*, Topics in Applied Physics, Vol. 101, edited by B. Hillebrands and A. Thiaville (Springer-Verlag, Berlin, 2006), pp. 57–103.

[23] G. Gubbiotti, S. Tacchi, M. Madami, G. Carlotti, A. O. Adeyeye, and M. Kostylev, J. Phys. D: Appl. Phys. **43**, 264003 (2010).